Geophysical Prospecting, 1994, 42, 755–776

Cost-effective 3D one-pass depth migration[1]

A. Sollid[2] and B. Arntsen[2]

Abstract

A crucial point in the processing of 3D seismic data is the migration step, both because of its 3D nature and the computational cost involved. The efficiency and accuracy of 3D migration are determined by the wavefield extrapolation technique employed. Wavefield extrapolation based on second-order differential operators of variable-length is very efficient and accurate at the same time. Compared to migration based on the McClellan transform and operator splitting, the use of variable-length second-order differential operators offers significant advantages. The 3D migration operator has an almost perfect circular symmetry. No positioning errors in the 45° azimuth between the in-line and cross-line directions are evident. The method is, in practice, only limited by spatial aliasing and does not require expensive interpolation of data to reduce numerical artifacts. This reduces the computational cost of 3D one-pass depth migration by a large factor.

Introduction

The 3D seismic method was first widely used in the late 1970s and early 1980s. Although an expensive method, the rewards in terms of increased drilling success rates have been very encouraging. A crucial point in processing of 3D seismic data is the migration step, both because of its 3D nature and the computational cost involved. Thus, it is desirable that the algorithms employed in the migration step are both accurate and effective. This paper describes an accurate and efficient method for 3D migration.

The use of effective migration algorithms is even more important when 3D prestack migration is considered. Promising results have been achieved in the imaging of subsalt fault systems by using 3D prestack migration methods based on asymptotic ray theory (Western and Ball 1992).

Since ray theory cannot adequately describe all aspects of seismic wave propagation, it is expected that a method based on the full wave equation will yield even better results than those obtained by ray theory. Development of 3D prestack migration methods based on the full wave equation is not straightforward due to the massive computational power required. Shot-record migration of a realistic

---

[1] Paper presented at the 55th EAEG meeting, Stavanger, June 1993. Received December 1993, revision accepted April 1994.

[2] Statoil Research Centre, Postuttak, 7005 Trondheim, Norway.

data set would be too time consuming using present-day technology. However, Rietveld, Berkhout and Wapenaar (1992) describe a promising method using plane-wave decomposition along the shot-axis requiring a computational effort equivalent to a relatively small number of 3D post-stack migrations. The 3D migration method described in this paper could be used in such a 3D prestack scheme.

A number of algorithms used in 2D depth migration have been difficult to extend to the 3D case. For instance the 45° finite-difference implicit migration scheme cannot be used effectively in 3D, since this method requires the solution of a large system of linear equations for each depth-step (Brown 1983). Instead, a large number of approximate techniques were developed, including two-pass migration (Gibson, Larner and Levin 1983) and the splitting method (Brown 1983). These methods have well-known problems in terms of positioning errors for the splitting method and problems with handling lateral velocity variations for the two-pass method.

Holberg (1988) proposed a new technique for 2D depth migration in the frequency–space domain based on optimized spatial convolutional operators. This technique is very accurate and cost-effective and is able to handle lateral velocity variations. Blaquière *et al.* (1989) extended this method to 3D in a straightforward way, obtaining an accurate but very expensive method for 3D migration. Hale (1991) introduced a similar but much more effective method for 3D migration based on the McClellan transform. The method of Hale (1991) is comparable to operator splitting in terms of efficiency, but avoids some of the large positioning errors in the 45° direction between the in-line and cross-line directions. However, this method is still computationally very demanding partly due to the dense computational grid required to avoid numerical dispersion. Blaquière (1991) improved on to the method devised by Hale (1991) by using optimized McClellan transforms. Recently Soubaras (1992) introduced a method closely related to that of Hale (1991), but based on an expansion of the wave extrapolator in second-order differential operators rather than employing the McClellan transform. Soubaras (1992) also used the Remez algorithm to design the coefficients for the expansion and the differential operators themselves. This method avoids the numerical dispersion to a large degree and is comparable in terms of computational cost.

In the present work Soubaras' (1992) expansion in second-order differential operators is used, but it is shown how the expansion coefficients and the differential operators can be designed using a least-squares approach rather than the Remez algorithm. Also the original method of Soubaras (1992) is improved upon by using a set of variable-length second-order differential operators. This set of operators has differing spectra and lengths to ensure that the resulting wave extrapolator is very effective and accurate at the same time.

The next two sections detail the theory of the design of wave extrapolators. Then follows a section on numerical implementation and a section with application to 3D migration. Finally, the computational cost is considered.

3D wavefield extrapolation

Depth extrapolation of a seismic wavefield from depth level z to depth level $z + \Delta z$ can be performed in the frequency–wavenumber domain with the phase-shift method (Gazdag 1978), i.e.

$$P(\omega, \hat{k}_x, \hat{k}_y, z + \Delta z) = W(\omega, \hat{k}_x, \hat{k}_y, \Delta z) P(\omega, \hat{k}_x, \hat{k}_y, z), \tag{1}$$

where $P(\omega, \hat{k}_x, \hat{k}_y, z)$ is the seismic wavefield at depth level z as a function of temporal frequency ω and the in-line and cross-line wavenumbers $\hat{k}_x$ and $\hat{k}_y$. The sampling interval in depth is denoted Δz. The phase-shift operator W is given by

$$W(\omega, \hat{k}_x, \hat{k}_y, \Delta z) = \exp\left\{ \mathrm{i}\, \Delta z \left[\left(\frac{\omega}{c} \right)^2 - \hat{k}_x^2 - \hat{k}_y^2 \right]^{1/2} \right\}, \tag{2}$$

where c is the wave-propagation velocity.

As is well known, the depth extrapolation described by (1) is only valid for a horizontally layered medium without lateral changes in the wave velocity. This restriction can be approximately relaxed by considering wave extrapolation in the frequency–space domain by a Fourier transform of (1) over the wavenumbers $\hat{k}_x$ and $\hat{k}_y$, such that

$$p(\omega, x, y, z = \Delta z) = w(\omega, x, y) * p(\omega, x, y, z). \tag{3}$$

The '$*$' operation denotes 2D convolution along the in-line and cross-line directions, and w is the inverse Fourier transform of the phase-shift operator given by (2). Lateral changes in wave velocity can be accommodated by allowing w to be space-variant. This can in practice be achieved by substituting w with space-variant convolutional operators f that are designed to fit the exact operator for a range of ω/c ratios. The operators f are optimized such that their Fourier transforms approximate the exact phase-shift operator given by (2).

3D wave extrapolators using second-order differential operators

In the description of the operator design we have preferred to normalize the wavenumbers $\hat{k}_x$ and $\hat{k}_y$ by the in-line and cross-line sampling interval Δx and Δy, such that

$$k_x = \hat{k}_x \, \Delta x$$

and

$$k_y = \hat{k}_y \, \Delta y. \tag{4}$$

It is assumed that the in-line and cross-line sampling intervals are equal. However, the method could, in principle, be generalized to allow different in-line and cross-line sampling intervals. The phase-shift function in (2) can be rewritten as

$$W(k_\omega, k_x, k_y) = \exp\left\{ \mathrm{i} \epsilon k_\omega \left[1 - 2 \left(\frac{k}{k_\omega} \right)^2 \right]^{1/2} \right\}, \tag{5}$$

where ϵ is equal to

$$\epsilon = \frac{\Delta z}{\Delta x}, \tag{6}$$

and the normalized local wavenumber k_ω is equal to

$$k_\omega = \frac{\omega \, \Delta x}{c}. \tag{7}$$

k is given by

$$k^2 = \tfrac{1}{2}(k_x^2 + k_y^2). \tag{8}$$

Note that k and the normalized wavenumbers k_x, k_y and k_ω are all defined in the interval $[0, \pi]$. The wavefield extrapolator given by (5) can now be completely specified by the parameters k_ω and ϵ.

The design of the extrapolation operator is done in the frequency–wavenumber domain in order to approximate the exact phase-shift operator in (5). In Appendix A, it is shown that the Fourier transform of the depth extrapolation operator f may be expressed as the expansion

$$F(k_\omega, k_x, k_y) = 2 \sum_{n=0}^{N} f_n H_n(k_\omega, k_x, k_y), \tag{9}$$

where f_n are complex coefficients and N is the half-length of the operator. The functions H_n are computed by using the recursive formula for Chebyshev polynomials (Rottmann 1960),

$$H_n = 2HH_{n-1} - H_{n-2}, \qquad n \geq 2, \tag{10}$$

where $H_0 = 1$ and $H_1 = \mathrm{H}$. This technique is described in detail in Appendix A. The function H is written as

$$H(k_\omega, k_x, k_y) = \beta_0 + \beta_1 \tfrac{1}{2}[D(k_\omega, k_x) + D(k_\omega, k_y)], \tag{11}$$

where D is the frequency response of a symmetrical finite impulse response (FIR) filter that approximates k_x^2 or k_y^2 for wavenumbers less than or equal to k_ω. With respect to k_x, it is expressed as

$$D(k_\omega, k_x) = 2 \sum_{l=0}^{L} u_l(k_\omega) \cos(lk_x), \tag{12}$$

where u_l are real coefficients and L is the operator half-length. The inverse Fourier transform d is an approximation to the ideal spatial second-order differential operator. It follows that H in (11) is the frequency response of a spatial convolutional operator h composed of two differential operators $d(x)$ and $d(y)$ applied along the in-line and cross-line direction, respectively. The operator h is therefore cross-shaped, as shown in Fig. 1. By using two orthogonal second-order differential operators in the design of h, the frequency response H will be almost perfectly

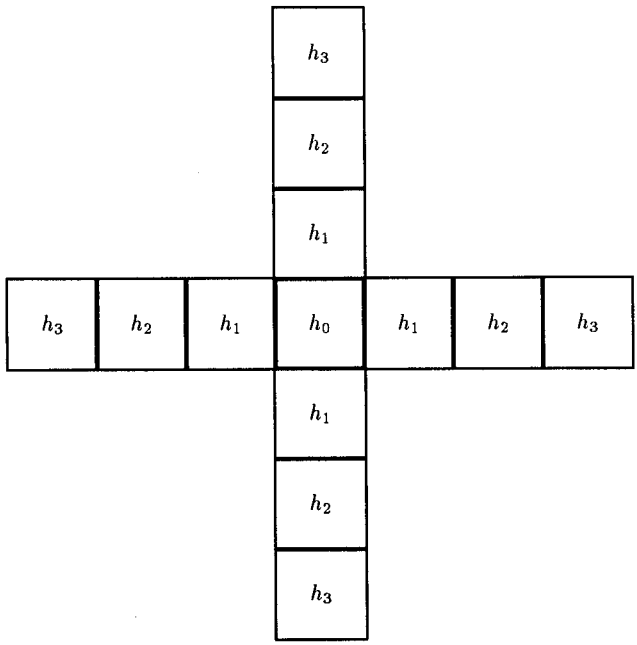

Figure 1. Layout of the filter $h(x, y)$ with length L equal to 3.

circularly symmetric for wavenumbers that correspond to propagating waves. The constants β_0 and β_1 (Soubaras 1992) in (11) are given by (A19) and (A20). They are chosen so that numerical stability is retained in the Chebyshev recursion.

Equations (9)–(12) contain one set of unknown complex coefficients, f_n, and another set of unknown real coefficients, u_l. Both sets of coefficients could, in principle, be determined simultaneously by a least-squares optimization procedure, but the differential operator coefficients u_l are related in a non-linear way to the response F, making least-squares optimization difficult. Instead, the problem is solved in two stages. The differential operator coefficients u_l are determined first by solving a least-squares optimization problem. Secondly, the optimized differential operator frequency response given by (12) is used in (11) to compute H, which is used to determine the complex coefficients f_n by another least-squares procedure.

Least-squares differential operator design

The second-order differential operator d is designed by chosing the coefficients u_l such that the difference between the Fourier transform D of d and the Fourier transform of the exact second-order differential operator is a minimum in a least-squares sense. This is expressed as minimizing the object function I with respect to

the coefficients u_l, i.e.

$$I = \sum_{k_x=0}^{k_\omega} \| D(k_\omega, k_x) - k_x^2 \|^2. \tag{13}$$

For a given accuracy, the shortest possible operator half-length L is chosen.

Least-squares 3D wave extrapolator design

The coefficients f_n of the wavefield extrapolator F given by (9) are determined by minimizing the object-function

$$\mathcal{J} = \sum_{k=0}^{k_\omega/\sqrt{2}} \| F(k_\omega, k) - W(k_\omega, k) \|^2, \tag{14}$$

with respect to the complex coefficients f_n subject to the constraint that $|F(k_\omega, k)| \leq 1$ for $|k| \leq \pi$. This constraint addresses the stability of the explicit operator. The maximum ripples in the amplitude response for $k \leq k_\omega/\sqrt{2}$ must be kept sufficiently small to guarantee accurate and stable extrapolation. For a given accuracy and maximum angle of propagation, the shortest possible operator half-length N is chosen. Note that the minimization of the object-function in (14) is effectively carried out in the 45° azimuth direction that corresponds to the particular combination $k = k_x = k_y$. The result is then used for all other combinations of k_x and k_y. This enables us to use optimization software originally designed for optimizing 2D migration operators with very little modification.

Numerical implementation

Using (3) with the approximate wavefield extrapolator f substituted for w, the equation to be implemented for depth extrapolation of the wavefield p is

$$p(\omega, x, y, z + \Delta z) = f(k_\omega, x, y) * p(\omega, x, y, z), \tag{15}$$

where f is given by the inverse spatial Fourier transform over k_x and k_y of (9), that is

$$f(k_\omega, x, y) = \sum_{n=0}^{N} f_n(k_\omega) h_n(x, y). \tag{16}$$

The overall scheme is similar to the recursion scheme used by Hale (1991) to implement wavefield extrapolation using the McClellan transform. It is shown schematically in a simplified form in Fig. 2. Equation (16) can easily be implemented by repeated application of the spatial filter $h(x, y)$ to the data p, combined with multiplication of the complex coefficients f_n.

As described in the previous section, the complex coefficients f_n and the real coefficients u_l of the second-order differential operators depend in general on the normalized local wavenumber. In principle, one would like to optimize these coef-

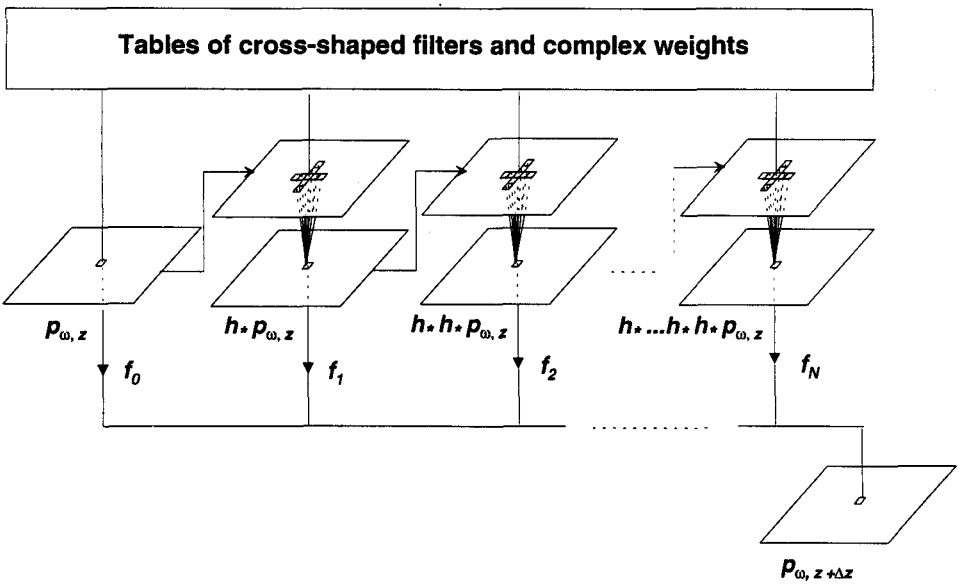

Figure 2. Computational scheme for the 3D migration based on second-order differential operators.

ficients for each normalized local wavenumber k_ω. However, an approach based on spatially variant differential operators is difficult to implement efficiently on vector machines due to memory problems. Blaquière (1991) has devised a technique that eliminates the implementation problems and still retains sufficient accuracy. He applied the technique to the McClellan transform method, but a similar scheme is applicable to depth extrapolation using (16): a limited number of second-order differential operators are optimized such that, for a given length L, the maximum wavenumber denoted $k_\omega^{\max}$ is as large as possible for a specified accuracy. Table 1 shows typical selected values of $k_\omega^{\max}$ for half-lengths L from one up to seven. The corresponding frequency responses of the differential operators are shown in Fig. 3. The coefficients can be computed once and for all and then be applied generally in the operator design.

Since the f_n coefficients depend on the second-order differential operators coefficients u_l through (14), a separate set of f_n coefficients are estimated for each set of second-order differential operator coefficients u_l. The set of complex coefficients

Table 1. The number of coefficients used in the second-order differential operators as a function of the maximum wavenumber.

$k_\omega^{\max}/\pi$	0.17	0.36	0.50	0.62	0.72	0.82	0.90
L	1	2	3	4	5	6	7

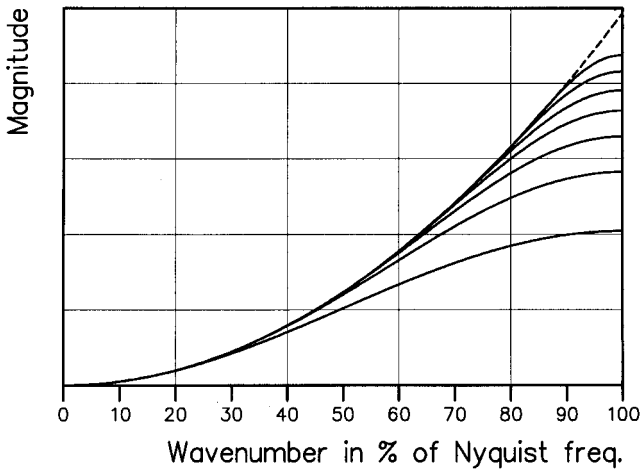

Figure 3. Frequency responses of seven second-order differential operators (solid lines) with half-length L decreasing from 7 to 1 (from top to bottom). The dashed line corresponds to the ideal second-order differential operator.

f_n is computed for all wavenumbers up to $k_\omega^{\max}$. The number of complex coefficients N is kept constant. The tables of coefficients are estimated once and stored in a file.

Prior to the wave extrapolation, the coefficients f_n are read into memory and linearly interpolated. The number of separate tables needed to store the complex coefficients is equal to the number of second-order differential operators used. For each depth slice (z-coordinate equal to a constant) in the extrapolation, the minimum velocity $c_{\min}$ must be found by scanning the velocity model. Given a frequency ω, the ratio $\omega \Delta x / c_{\min}$ decides the correct operator table and differential operator to be applied. The normalized local wavenumber k_ω, divided by the discretization interval Δk_ω, is used as an index for the actual table of complex coefficients.

Figure 4 shows contours of the frequency response of $h(x, y)$ as a function of the wavenumbers k_x and k_y for $L = 7$. The bold lines are the frequency response of $h(x, y)$, while the thin lines are the ideal circularly symmetric response. The frequency response is reasonably accurate, at least up to 90% of the Nyquist limit.

As mentioned above, Hale (1991) described a method for 3D wave extrapolation based on the McClellan transform. The expression for the wavefield extrapolator F due to Hale (1991) is given in Appendix B and is similar to (9), with the main difference being a different expression for the function H. The inverse Fourier transform of Hale's H function is a filter with 17 points. The filter is fixed and is not optimized with respect to the local wavenumber. Figure 5 shows contours of the frequency response of this filter as a function of the wavenumbers k_x and k_y. Comparing the response (bold lines) with the exact response (thin lines), it can be

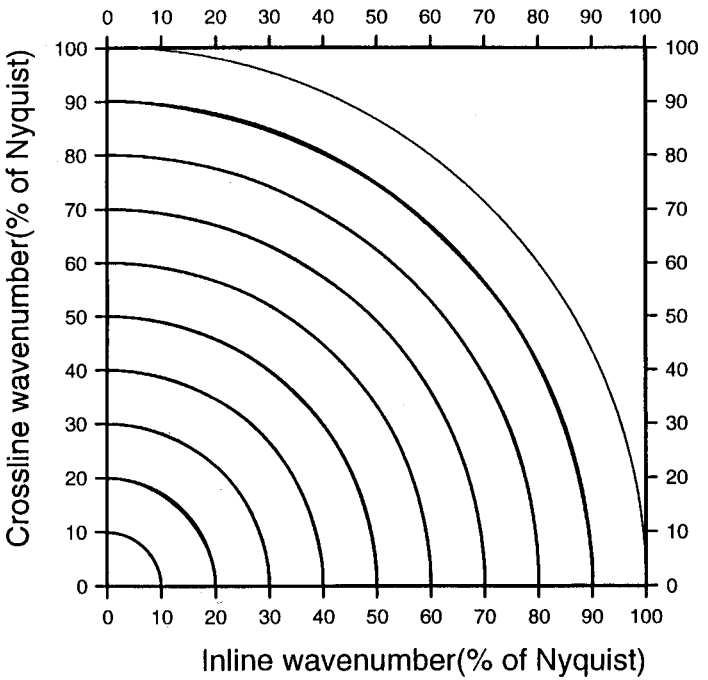

Figure 4. Contours of constant k for $h(x, y)$ based on a second-order differential operator with $L = 7$ (bold lines) compared to the ideal circular response (thin lines).

seen that the filter response already starts to deviate from the ideal response at wavenumbers equal to half the Nyquist limit. Comparing Figs 4 and 5, it is clear that the approach based on second-order differential operators is significantly more accurate for high wavenumbers.

Application to 3D migration

The wavefield extrapolators described in the previous section are very suitable for application to 3D post-stack migration. The following four methods for 3D post-stack migration are tested and compared.

1. 3D migration based on variable-length second-order differential operators.
2. 3D migration based on a fixed second-order differential operator.
3. 3D migration based on the improved McClellan transform method as described by Hale (1991).
4. 3D migration based on the splitting approximation as described by Brown (1983).

For the 3D migration based on variable-length second-order differential operators, we used the design approach described in the previous section. The number of complex coefficients N in the expansion of the extrapolation operator was kept

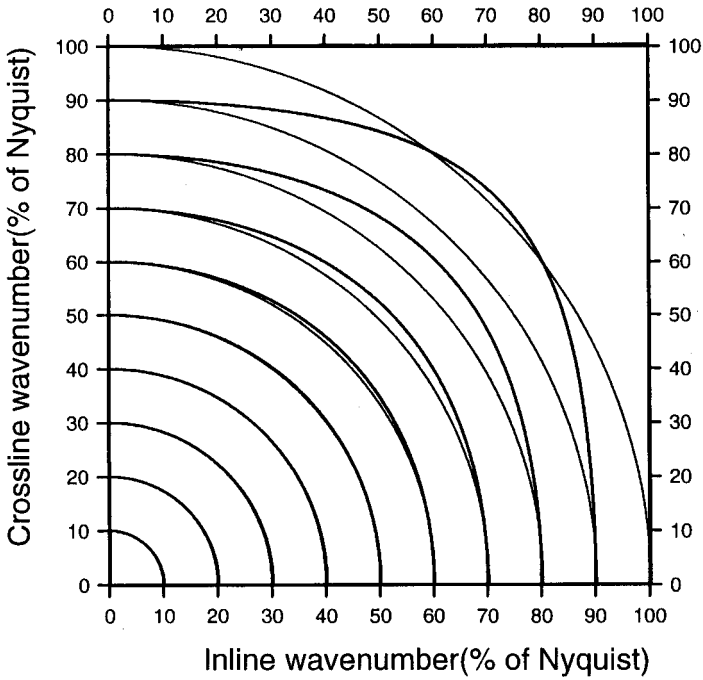

Figure 5. Contours of constant k for $h(x, y)$ based on Hale's improved McClellan transform (bold lines) compared to the ideal circular response (thin lines).

constant and equal to 19. The h function used filters of half-length L ranging from $L = 1$ to 7. The 3D migration based on a fixed second-order differential operator used the same approach as described for the optimized operator, except that the length L was kept constant and equal to 6, and that the coefficients were fixed. The accuracy of this operator was reasonable up to $k_\omega^{\max} = 0.85\pi$. The 3D migration based on the McClellan transform method was based on Hale's improved 17-point filter for the h function. The number of complex coefficients was equal to 19 and was designed using Holberg's (1988) method for 2D wave extrapolators. For the 3D migration based on the splitting method, the same 2D operator was used. The splitting method consists of applying 2D extrapolation in the x-direction for all y, followed by extrapolation in the y-direction for all x for each depth level.

The input data consisted of a single band-limited spike located at $x = 0$, $y = 0$ and time 0.9 seconds. The largest frequency component in the input data was 50 Hz, while the spatial sampling intervals were $\Delta x = \Delta y = 10$ m. The temporal sampling interval was $\Delta t = 10$ ms and the velocity was equal to 2000 m/s. The numerical examples shown thus involve wavenumbers up to the Nyquist limit.

Figures 6, 7, 8 and 9 show horizontal cross-sections at depth $z = 350$ m of the migrated images for the 3D migration based on variable-length second-order dif-

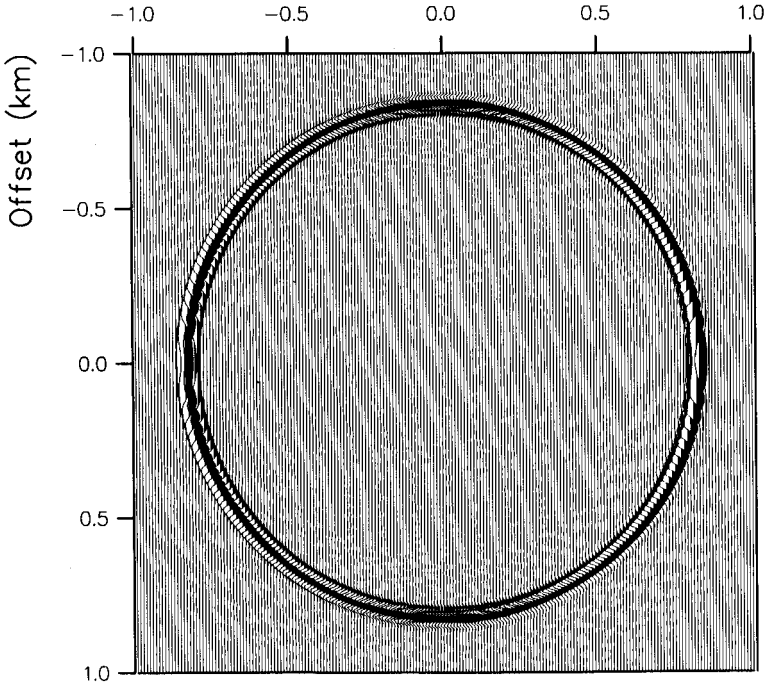

Figure 6. Impulse response of 3D migration based on variable-length second-order differential operators at depth $z = 350$ m.

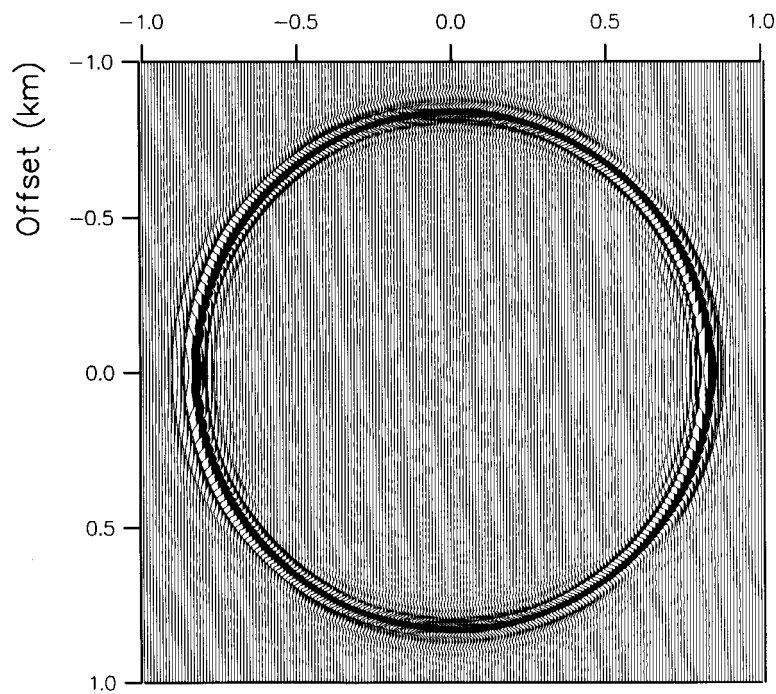

Figure 7. Impulse response of 3D migration based on a fixed second-order differential operator at depth $z = 350$ m.

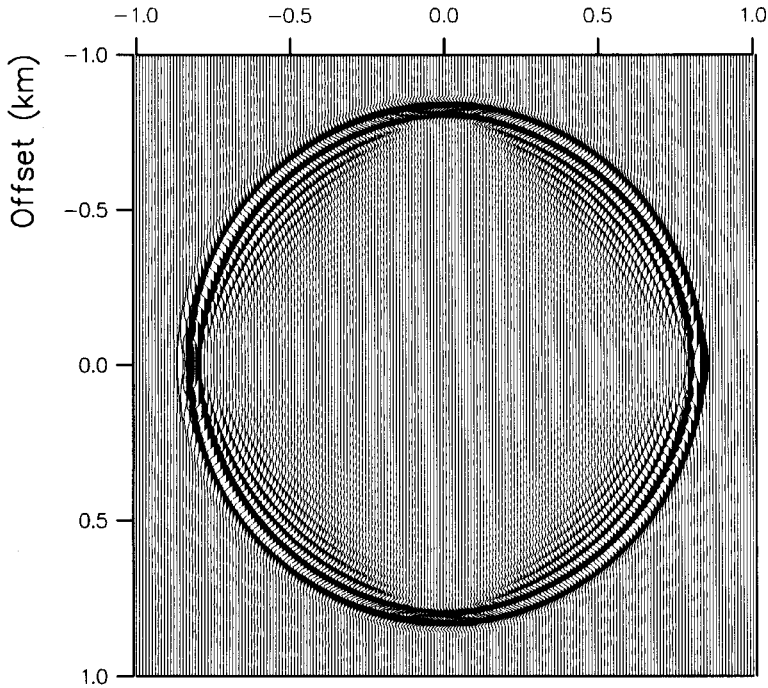

Figure 8. Impulse response of 3D migration based on Hale's improved McClellan transform at the depth $z = 350$ m.

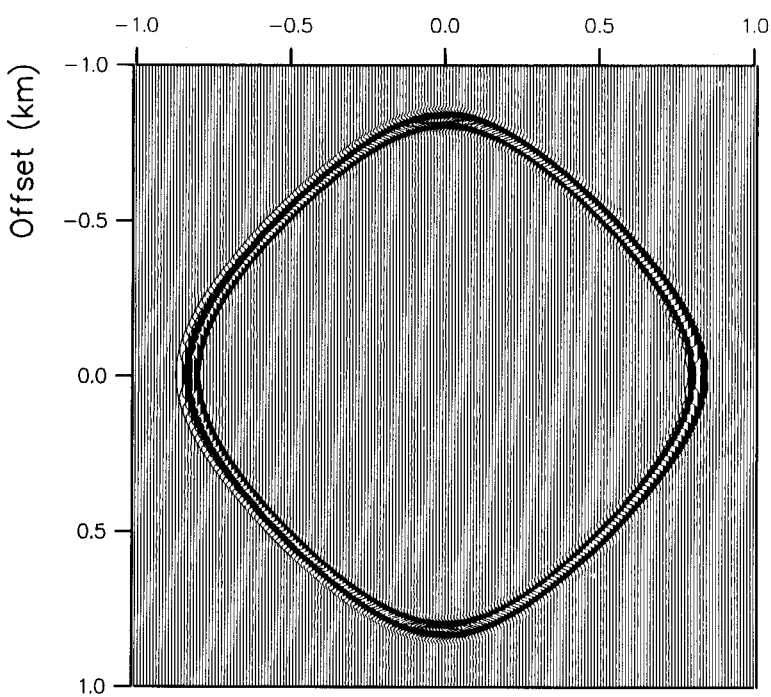

Figure 9. Impulse response of 3D migration based on splitting at depth $z = 350$ m.

ferential operators, 3D migration based on a fixed second-order differential operator, 3D migration based on the improved McClellan transform and the splitting method, respectively. Figures 10, 11, 12 and 13 show the vertical cross-sections.

The 3D migration based on a fixed second-order differential operator yields more numerical dispersion in the in-line and cross-line directions than the 3D migration based on variable-length second-order differential operators, as is evident when comparing Figs 7 and 11a with Figs 6 and 10a. The numerical artifacts are due to the fact that the applied second-order differential operator is not sufficiently accurate. By increasing the length of the second-order differential operator, and thus increasing the computational cost, the artifacts can be reduced.

Comparing Figs 6 and 8, it is seen that the McClellan transform method exhibits considerable artifacts due to numerical dispersion. This is particularly evident in

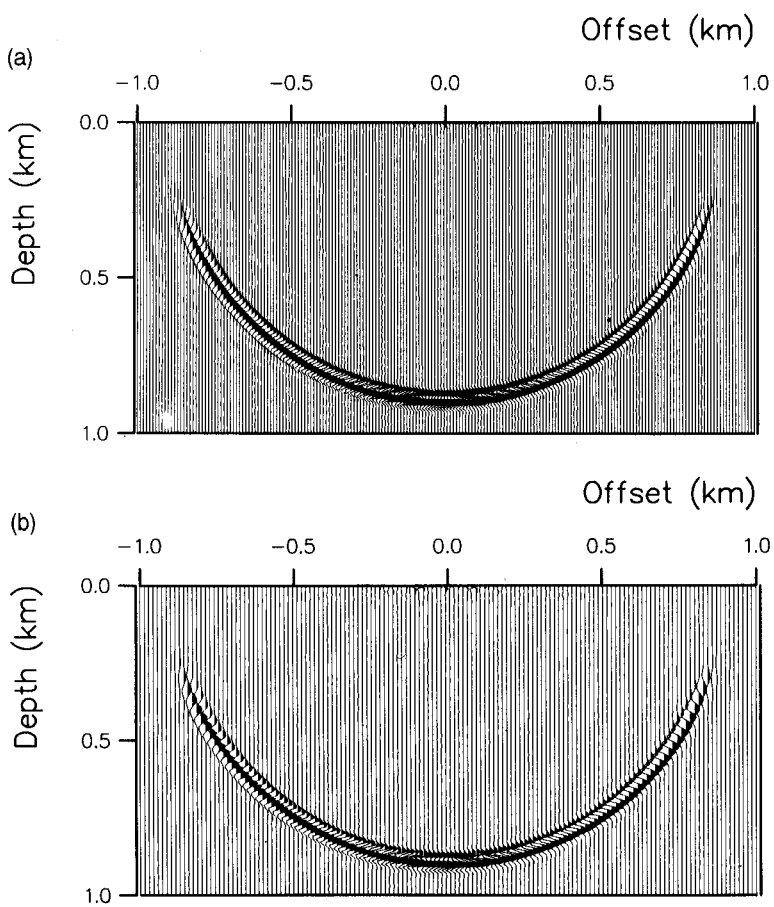

Figure 10. Impulse response of 3D migration based on variable-length second-order differential operators taken (a) in the in-line direction at $y = 0$ and (b) diagonally between the in-line and cross-line directions ($x = y$).

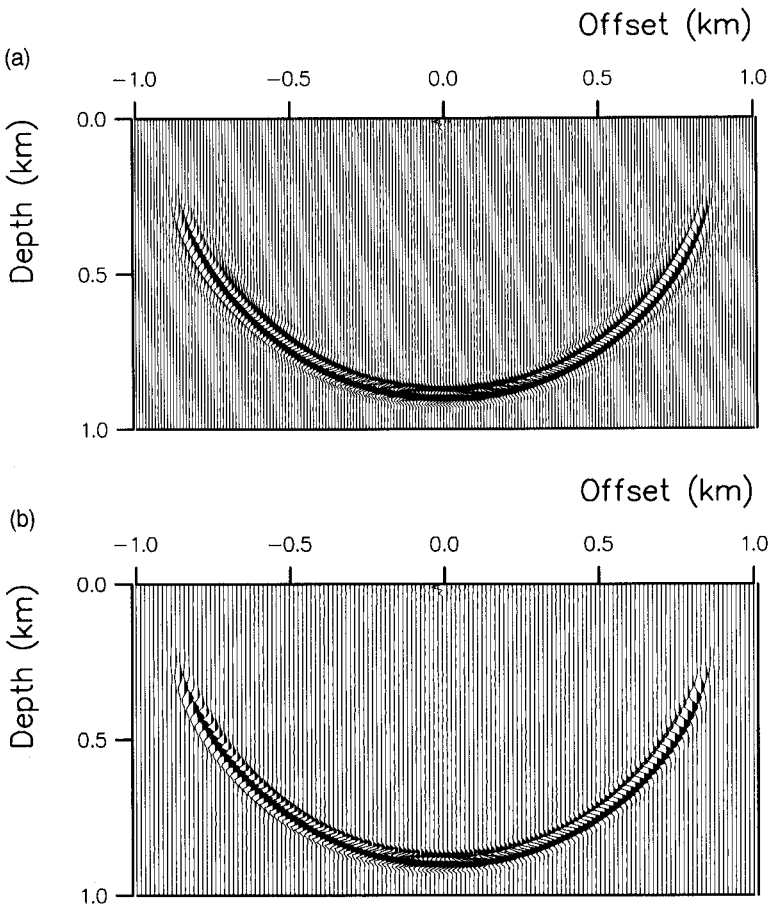

Figure 11. Impulse response of 3D migration based on a fixed second-order differential operator taken (a) in the in-line direction at $y = 0$ and (b) diagonally between the in-line and cross-line directions ($x = y$).

the 45° azimuth between the in-line and cross-line directions, as can be seen in Fig. 12b. The numerical dispersion seen in the 3D migrated image when using the McClellan transform method can be understood by considering Fig. 5. The contours of the 2D h-filter show the largest deviation with increasing k for $k_x \approx k_y$.

Comparing Figs 6 and 9, the splitting method is seen to exhibit large positioning errors, particularly in the 45° azimuth between the in-line and cross-line directions.

Computational cost

Due to the simple cross-shaped filters h of variable size and the application of the recursive Chebyshev structure, the scheme is very efficient. The number of

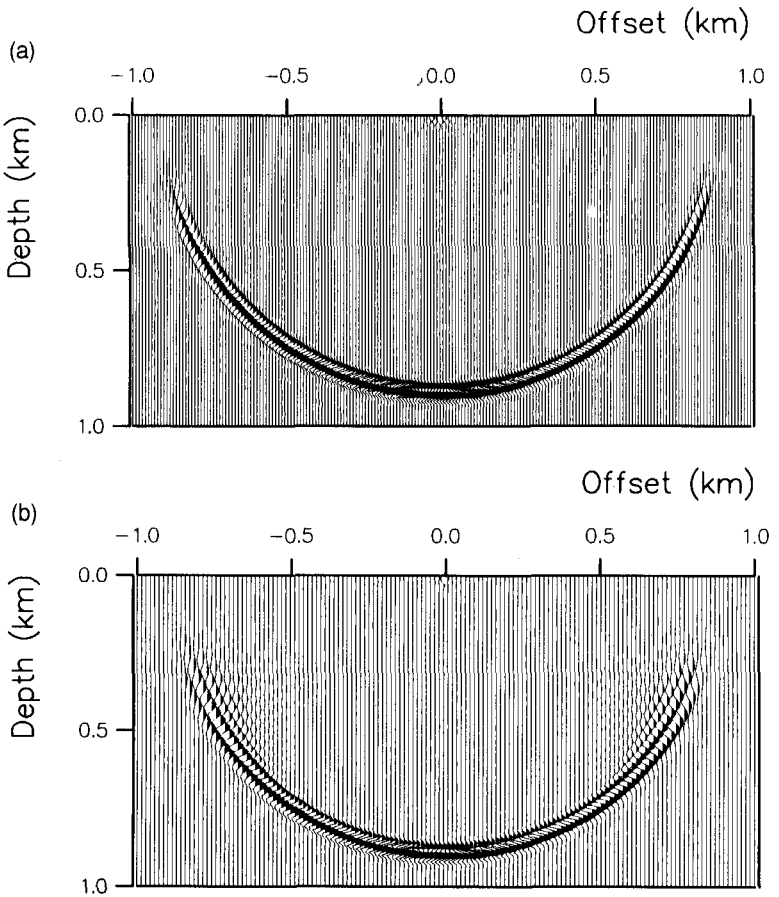

Figure 12. Impulse response of 3D migration based on Hale's improved McClellan transform taken (a) in the in-line direction at y = 0 and (b) diagonally between the in-line and cross-line directions ($x = y$).

floating-point operations for each grid point q expressed as a function of the number of complex coefficients N and the number of differential operator coefficients L, is estimated to be

$$q(N, L) = N[10L + 12] + 6. \tag{17}$$

For a 70° operator, we apply differential operators of half-lengths L ranging from $L = 1$ to 7, and the mean value of L is estimated to be 3.6. For $L \approx 3.6$, (17) reduces to

$$q(N) \approx 48N. \tag{18}$$

Note that in practice this function expresses the worst case. Figure 14 illustrates this: as the velocity tends to increase with depth, the average half-length L and the

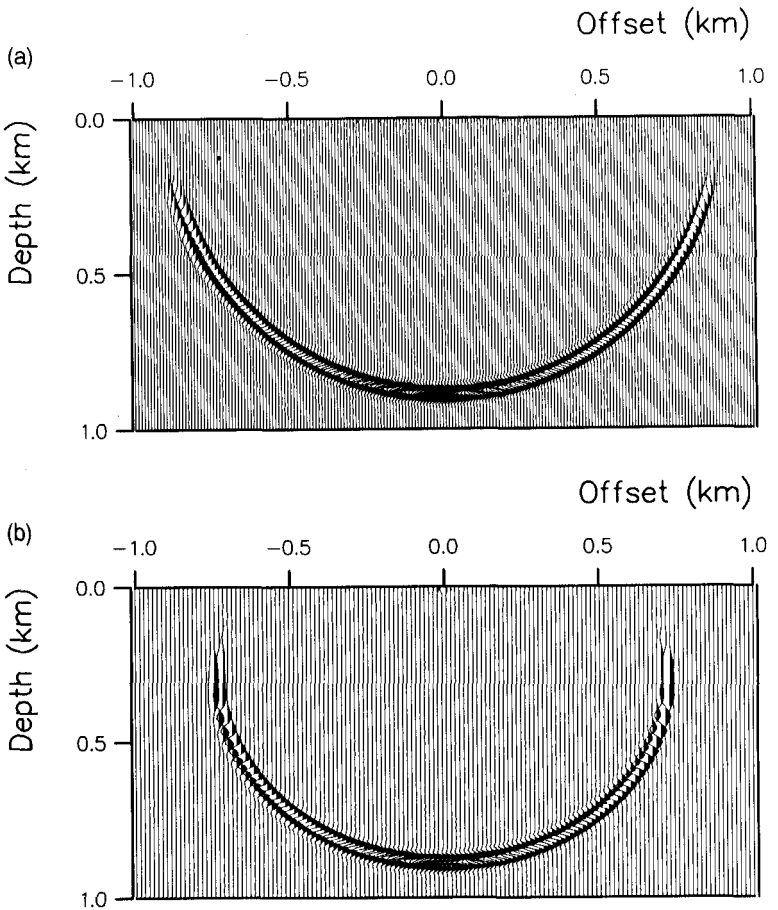

Figure 13. Impulse response of 3D migration based on splitting taken (a) in the in-line direction at $y = 0$ and (b) diagonally between the in-line and cross-line directions ($x = y$).

computational cost will be reduced significantly. This is due to the fact that for waves dominated by small wavenumbers, mainly small-sized differential operators are used. Furthermore, Fig. 14 shows that 3D migration based on a fixed second-order differential operator is more expensive than 3D migration based on optimized second-order differential operators.

The corresponding expression for the scheme proposed by Hale (1991), using the improved McClellan transform is

$$r(N) = 52N + 6. \tag{19}$$

For comparison, the corresponding expression for operator splitting is

$$s(N) = 20N + 12. \tag{20}$$

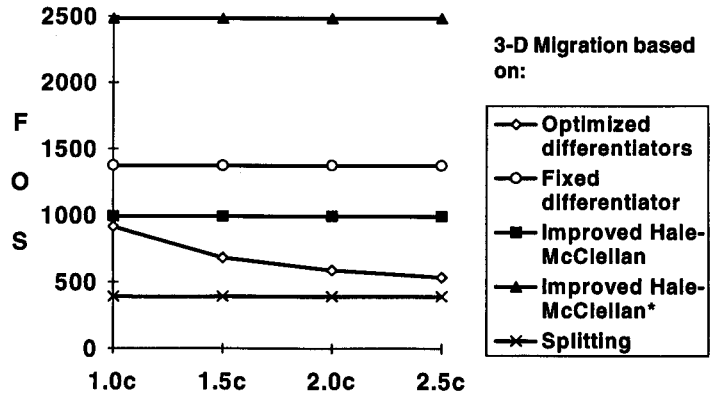

Figure 14. Computational cost for the 3D migration methods used in the numerical examples. The cost is measured in floating point operations per output sample (FOS) as a function of the lowest velocity c allowed in the model predicted by the Nyquist limit. In addition, the 'equivalent' number of FOS for the improved Hale–McClellan method is shown (marked '*'), where we have assumed a denser computational grid with 2.5 times as many grid points as used in the other methods.

From (18), (19), (20) and Fig. 14, it is seen that the scheme based on variable-length differential operators is slower than operator splitting, but somewhat faster than the improved McClellan transform. However, as was shown in the previous section, the scheme based on variable-length differential operators is significantly more accurate than both the improved McClellan scheme and operator splitting.

From the numerical examples it is evident that the 3D migration based on second-order variable-length differential operators, is, in practice, only limited by spatial aliasing, and not by numerical dispersion. Compared to 3D migration based on the McClellan transform method, this offers a significant advantage in terms of computational cost. For 3D migration based on the McClellan transform method to perform well on the example shown in Figs 6 to 13, it would have been necessary to use a larger number of grid points per shortest wavelength. This results in an increase of the computational load by a factor of approximately 2.5 compared to 3D migration based on second-order differential operators. This is shown clearly in Fig. 14.

Conclusions

It has been shown how an accurate 3D wave extrapolation operator can be expressed as an expansion in second-order differential operators. The expansion is similar to an expansion derived by Soubaras (1992), but uses variable-length differential operators and a least-squares design approach. The method has the following advantages:

1. The 3D wavefield extrapolator is almost perfectly circularly symmetric.

2. The problem of numerical dispersion for high wavenumbers is avoided. The method is thus limited only by spatial aliasing and not by numerical dispersion.
3. A coarse computational grid can thus be used. Compared to the McClellan transform method, this translates into reduction in the computational load by a factor of more than two.

The use of variable-length second-order differential operators is essential, as the use of a fixed second-order differential operator leads to more numerical disperson or to a significantly higher computational cost.

Considering future application to full-wave prestack 3D depth migration, it is essential to use a highly effective wave extrapolation algorithm. A scheme with variable-length second-order differential operators ensures both correct wave extrapolation and efficiency.

Acknowledgements

We are grateful to Olav Holberg, Lasse Amundsen and John R. Granli for stimulating discussions. Dr Holberg initially suggested the problem and provided some of the software for the least-squares operator design.

Appendix A

Series expansion of the 3D phase-shift operator

In this appendix it is shown how the 3D phase-shift operator is given by (5) can be written as a series expansion in powers of the horizontal normalized wavenumbers k_x and k_y. Equation (5) reads

$$W(k_\omega, k_x, k_y) = \exp\left\{\epsilon k_\omega\left[1 - 2\left(\frac{k}{k_\omega}\right)^2\right]^{1/2}\right\}, \tag{A1}$$

where

$$k_\omega = \frac{\omega\,\Delta x}{c}, \tag{A2}$$

$$k^2 = \tfrac{1}{2}(k_x^2 + k_y^2) \tag{A3}$$

and

$$\epsilon = \Delta z/\Delta x. \tag{A4}$$

A Taylor expansion of the phase-shift operator in (A1) leads to the expression

$$W(k_\omega, k_x, k_y) = \sum_{n=0}^{\infty}\left\{i\epsilon k_\omega\left[1 - 2\left(\frac{k}{k_\omega}\right)^2\right]^{1/2}\right\}^n \frac{1}{n!}. \tag{A5}$$

Using the series expansion (Rottman 1960)

$$(1-2x)^{n/2} = 1 - nx + \frac{n(2-n)}{2!}x^2 + \cdots,$$
$$= \sum_{m=0}^{\infty} a_m x^m, \tag{A6}$$

where

$$a_m = (-1)^m \frac{n(2-n)(4-n)\ldots[(m-1)2-n]}{m!}, \tag{A7}$$

in (A5) and substituting $x = (k/k_\omega)^2$, we get

$$W(k_\omega, k_x, k_y) = \sum_{n=0}^{\infty} \left\{ \frac{(\mathrm{i}\epsilon k_\omega)^n}{n!} \left[\sum_{m=0}^{\infty} a_m \left(\frac{k}{k_\omega} \right)^{2m} \right] \right\}. \tag{A8}$$

Equation (A8) may be rearranged as

$$W(k_\omega, k_x, k_y) = \sum_{m=0}^{\infty} \left\{ k^{2m} \left[\sum_{n=0}^{\infty} \frac{a_m}{k_\omega^{2m}} \frac{(\mathrm{i}\epsilon k_\omega)^n}{n!} \right] \right\}. \tag{A9}$$

By defining coefficients γ_m as

$$\gamma_m(\epsilon k_\omega) = \sum_{n=0}^{\infty} \frac{a_m}{k_\omega^{2m}} \frac{(\mathrm{i}\epsilon k_\omega)^n}{n!}, \tag{A10}$$

(A9) may be written as

$$W(k_\omega, k_x, k_y) = \sum_{m=0}^{\infty} \gamma_m(\epsilon k_\omega) k^{2m}. \tag{A11}$$

Equation (A11) is important since it shows that the phase-shift operator W given by (A1) can be expressed as an expansion in even powers of the normalized 'wave-number' k.

It is desirable to rewrite (A11) as an expansion in terms of cosines. We first express γ_m as

$$\gamma_m(\epsilon k_\omega) = 2 \sum_{n=0}^{\infty} \omega_n(\epsilon k_\omega)(-1)^m \frac{(n)^{2m}}{m!}, \tag{A12}$$

by the choice of suitable coefficients w_n. By substituting (A12) into (A11) and rearranging we get

$$W(k_\omega, k_x, k_y) = 2 \sum_{n=0}^{\infty} w_n(\epsilon k_\omega) \sum_{m=0}^{\infty} (-1)^m \frac{(nk)^{2m}}{m!}, \tag{A13}$$

$$W(k_\omega, k_x, k_y) = 2 \sum_{n=0}^{\infty} w_n(\epsilon k_\omega) \cos(nk). \tag{A14}$$

Equation (A12) shows that the coefficients w_n are a function of the local wavenumber k_ω, regarding ϵ as a constant i.e.

$$w_n = w_n(k_\omega). \tag{A15}$$

An approximation to W can be derived as follows: By truncating the right-hand side of (A13) after N terms we get

$$W(k_\omega, k_x, k_y) \approx 2 \sum_{n=0}^{N} w_n(k_\omega) \cos(nk). \tag{A16}$$

Equation (A16) is computationally advantageous since $\cos(nk)$ can be computed recursively by the Chebyshev recursion

$$\cos(nk) = 2 \cos k \cos[(n-1)k] - \cos[(n-2)k]. \tag{A17}$$

$\cos(k)$ can be approximated in the interval $[0, \pi]$ by the expression (Soubaras 1992)

$$\cos(k) \approx H(k) = \beta_0 + \beta_1 D(k), \tag{A18}$$

where $D(k)$ is an approximation to k^2. The coefficient β_0 is given by

$$\beta_0 = (D_{\max} + D_{\min})/(D_{\max} - D_{\min}), \tag{A19}$$

and β_1 is given by

$$\beta_1 = -2/(D_{\max} - D_{\min}). \tag{A20}$$

Here $D_{\min}$ and $D_{\max}$ are the minimum and maximum magnitudes of $D(k)$, respectively. Equation (A18) is a desirable expression since k^2 according to (A3) separates into independent terms for k_x^2 and k_y^2 which can be approximated by $D(k_x)$ and $D(k_y)$, giving

$$H(k) = \beta_0 + \beta_1 \tfrac{1}{2}[D(k_x) + D(k_y)]. \tag{A21}$$

Inserting (A21) into (A17) we get a recursive expression for H:

$$H(nk) = 2H(k)H[(n-1)k] - H[(n-2)k], \qquad n \geq 2. \tag{A22}$$

Now, using $H(nk)$ in (A16) instead of cos(nk) and optimizing w_n in a least-squares sense, we get

$$F(k_\omega, k_x, k_y, \Delta z) = 2 \sum_{n=0}^{N} f_n(k_\omega) H(nk), \tag{A23}$$

which approximates to W in (A1).

By an inverse Fourier transform of (A23) over the wavenumbers k_x and k_y, the frequency–space domain expression f for F is

$$f(k_\omega, x, y, \Delta z) = \sum_{n=0}^{N} f_n(k_\omega) h_n(x, y), \tag{A24}$$

where

$$h_n(x, y) = 2h(x, y) * h_{n-1}(x, y) - h_{n-2}(x, y), \qquad n \geq 2, \tag{A25}$$

and

$$h_0(x, y) = \delta(x)\delta(y), \qquad h_1(x, y) \equiv h(x, y). \tag{A26}$$

The '$*$' operation denotes 2D convolution along the x- and y-directions. h is the inverse Fourier transform of (11) over k_x and k_y :

$$h(x, y) = \beta_0 + \beta_1 \tfrac{1}{2}[d(x) + d(y)]. \tag{A27}$$

Here, the Fourier transforms of $d(x)$ and $d(y)$ are least-squares approximations to the normalized second-order differential operators k_x^2 and k_y^2. The spatial impulse responses are written as (Holberg 1987)

$$d(x) = \sum_{l=0}^{L} u_l[\delta(x - \Delta x) + \delta(x + \Delta x)], \tag{A28}$$

$$d(y) = \sum_{l=0}^{L} u_l[\delta(y - \Delta y) + \delta(y + \Delta y)]. \tag{A29}$$

The coefficients u_l are real valued.

Appendix B

Relationship with the McClellan transform method

In the following it is shown how the McClellan transform method as described by Hale (1991) can be obtained from the series expansion of the 3D phase-shift operator.

The McClellan transform method mainly consists of applying the same derivation as outlined in Appendix A. The phase-shift operator is written as

$$W(k_\omega, k_x, k_y) = \exp\left\{i\epsilon k_\omega\left[1 - 2\left(\frac{k}{k_\omega}\right)^2\right]^{1/2}\right\}. \tag{B1}$$

Proceeding as in Appendix A up to (A17), but instead of approximating $\cos(k)$ with a second-order polynomial in k, the following approximation is used (Hale 1991):

$$\cos(\sqrt{2}k) = \cos(\sqrt{k_x^2 + k_y^2}) \approx H'(k) = -1 + \tfrac{1}{2}(1 + \cos(k_x))(1 + \cos(k_y)) - \frac{c}{2}(1 - \cos 2k_x)(1 - \cos 2k_y). \tag{B2}$$

c is equal to 0.0255. The expression for the extrapolation operator f' is of the same form as that given in (16),

$$f'(k_\omega, x, y) = \sum_{n=0}^{N} f'_n(k_\omega)h'_n(x, y), \tag{B3}$$

but with h' equal to the inverse Fourier transform of (B2). The coefficients f'_n are the same as those applied in 2D migration.

References

Blacquière G. 1991. Optimized McClellan transformation filters applied in one-pass. 61st SEG meeting, Houston, USA., Expanded Abstracts, 1126–1129.

Blacquière G., Debeye H.W.J., Wapenaar C.P.A. and Berkhout A.J. 1989. 3D table-driven migration. *Geophysical Prospecting* **37**, 925–958.

Brown D.L. 1983. Applications of operator separation in reflection seismology. *Geophysics* **48**, 288–294.

Gazdag J. 1978. Wave-equation migration with the phase shift method. *Geophysics* **43**, 1342–1351.

Gibson, B., Larner K. and Levin S. 1983. Efficient 3-D migration in two steps. *Geophysics* **31**, 1–33.

Hale D. 1991. 3-D depth migration via McClellan transformations *Geophysics* **56**, 1778–1785.

Holberg O. 1987. Computational aspects of the choice of operator and sampling interval for numerical differentiation in large-scale simulation of wave phenomena. *Geophysical Prospecting* **35**, 629–655.

Holberg O. 1988. Towards optimum one-way wave propagation. *Geophysical Prospecting* **36**, 99–114.

Rietveld W.E.A., Berkhout A.J. and Wapenaar C.P.A. 1992. Optimum seismic illumination of hydrocarbon reservoirs. *Geophysics* **57**, 1334–1345.

Rottman K. 1960 Mathematische Formelsammlung. Bibliographisches Institut AG.

Soubaras R. 1992. Explicit 3-D migration using equiripple polynomial expansion and Laplacian synthesis 62nd SEG meeting, New Orleans, USA., Expanded Abstracts, 905–908.

Western, P.G. and Ball G.J. 1992. 3D prestack depth migration in the Gulf of Suez: a case history. *Geophysical Prospecting* **40**, 379–402.